J Inorg Organomet Polym
DOI 10.1007/s10904-017-0598-5

Wet Chemical Co-precipitation Synthesis of Nickel Ferrite Nanoparticles and Their Characterization

M. B. Tahir[1] · T. Iqbal[1] · A. Hassan[1] · Snobia Ghazal[1]

Received: 28 April 2017 / Accepted: 5 June 2017

Abstract In this study, wet chemical co-precipitation method was employed for the synthesis of pure and doped nickel ferrite nanoparticles at low temperature whereas the concentration of nickel varies from 2, 4, 6 and 8%. Optical absorption and transmission, Surface morphology, and structural properties of material are characterized by Fourier-transform infrared spectrometer, ultra-violet visible spectroscopy, scanning electron microscopy and powder X-ray diffraction respectively. It is observed that the transmission, size and band gap energy increases by increasing the amount of nickel. Red shift of the peaks is observed in the UV–visible spectra which is associated with the increase in size of the nickel ferrite. It can be used to fabricate devices intended to store data, for the classification of inorganic materials which plays a very important role in the different aspects of life due to their outstanding magnetic, electronic and optical properties.

Keywords Nanoparticles · Concentration · Nickel · Inorganic materials

1 Introduction

Metallic ferrite is the point of attention of researchers due to their extraordinary properties like magnetic, optical, chemical and electronic [1–4]. Metallic ferrites are chemically represented by the formula unit MFe_2O_4. M is a divalent metal ion such as Co^{2+}, Zn^{2+}, Fe^{2+}, Mg^{2+}, Ni^{2+}, Cd^{2+}, Cu^{2+} or a combination of these ions. Iron oxide nanoparticles having different kinds like hematite (α-Fe_2O_3), magnetite (Fe_3O_4), maghemite (γ-Fe_2O_3). These magnetic particles are used as a carrier of medicine in the body [5], treatment of cancer [6], magnetic resonance imaging and as a sensor [7].

Nickel ferrite shows soft ferromagnetic behavior is the form of bulk material [8]. They are known as cubic ferrites because most of the spinel ferrites form cubic spinel structure. Nickel substituted ferrite nanoparticles are magnetic particles used in various field of life. Nickel ferrite nanoparticles have inverse spinal structure with 32 octahedral as well as 64 tetrahedral sites. When Ni added in ferrite then octahedral sites contains Ni^{2+} and tetrahedral (A) sites as well as octahedral (B) sites contains Fe^{3+} [6, 9]. Nickel ferrite nanoparticles are the magnetic particles having extraordinary properties which can be used in several optical, magnetic, technological [10–12] and medical objectives. Nickel ferrite nanoparticles can be used as a device to store data [13] for the classification of inorganic materials which play a very important role in the different aspects of life due to their outstanding magnetic, electronic [14, 15] and optical properties. Nickel ferrite can be used in biomedical material and as a soft magnet [16] as multilayer chip inductor (MLCI), rod antenna, digital tape recording disks [17] and sensor device for humidity [18] drug delivery [19] inside the body thorough blood. As nickel ferrite particles are stable and have very high electrical resistivity due to which they can be used for as magnetic refrigerator [20]. It can also be commonly used as photo catalyst [21] for color imaging [22] magnetic resonance imaging [23, 24] as low loss materials at frequency [25].

Properties and particle size of the nano composites [26] can be controlled by different synthesis methods. Variety of techniques have been used like co-precipitation method

✉ M. B. Tahir
m.bilaltahir@uog.edu.pk

[1] Department of Physics, Faculty of Science, University of Gujrat, Hafiz Hayat Campus, Gujrat 50700, Pakistan

Published online: 22 June 2017

[27–33] sol–gel [30, 34–39] hydrothermal [40–42] solvothermal [22] oxidative polymerization [43] etc [16, 20, 44–46] physical [47] and biosynthesis [48] for the fabrication of nickel ferrite nanoparticle. Most of the mentioned method required hard conditions like very high temperature. Some methods are very slow required so much time to complete the reaction, toxic chemical involved etc. The substitution of the nickel control the particle size of the ferrite nanoparticle and change the structure of the particles. The concentration of the nickel in ferrite nanoparticles effects directly on the band gape of the ferrite nanoparticles. The absorption of the ferrite nanoparticles increases with the addition of nickel concentration.

This paper includes the fabrication of the nickel ferrite nanoparticles by suitable, easy and cost effective wet chemical co-precipitation method at low temperature. The effect of metal loading ferrite has been investigating with different parameters.

2 Material and Method

2.1 Synthesis of Pure Magnetic Ferrite Nanoparticles

Magnetic nanoparticles were prepared by wet chemical co-precipitation method. The precursor used for the synthesis of pure ferrite nanoparticles is ferric chloride ($FeCl_3{\cdot}6H_2O$) along with sodium hydroxide as precipitating agent. Ethanol (C_2H_6O) and distilled water are used for washing the precipitates.

Schematic diagram for the synthesis of pure ferrite nanoparticles in which ferric chloride ($FeCl_3{\cdot}6H_2O$) of 3.244 g (0.4 M) was measured in a 50 ml glass beaker whereas 2.99 g (3 M) of sodium hydroxide (NaOH) was measured in 25 ml beaker. Sodium hydroxide was dropped in the solution of the ferric chloride drop wise for 40 min at the constant temperature of 80 °C with constant stirring on magnetic stirrer. The pH of the solution should be >12. Filter the prepared precipitate by filter paper and dried by constant temperature oven by overnight. After drying precipitates were annealed at 600 °C for 6 h. Then we get pure magnetic ferrite nanoparticles (Fig. 1).

2.2 Synthesis of Nickel Ferrite Nanoparticles

Magnetic nickel ferrite nanoparticles were prepared with the same technique which is wet chemical co-precipitation. The precursors for the synthesis of nickel ferrite nanoparticles are ferric chloride ($FeCl_3{\cdot}6H_2O$), nickel chloride ($NiCl_2{\cdot}6H_2O$) along with the sodium hydroxide (NaOH) used as precipitating agent. Ethanol (C_2H_6O) and distilled water are used for washing the precipitates. Nickel ferrite nanoparticles are synthesized with different concentration

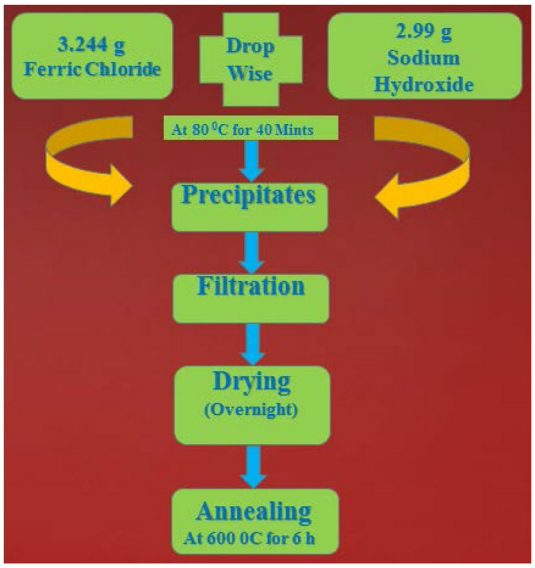

Fig. 1 Schematic diagram for the synthesis of pure ferrite nanoparticles

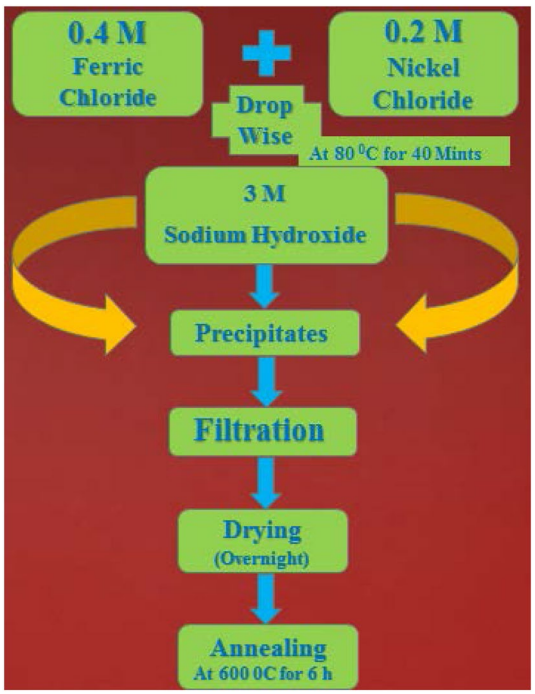

Fig. 2 Schematic diagram for the synthesis of nickel ferrite nanoparticles

of the nickel like 2, 4, 6 and 8% in magnetic ferrite nanoparticles.

Figure 2 shows the schematic diagram to synthesis the nickel ferrite nanoparticles in which ferric chloride ($FeCl_3{\cdot}6H_2O$) and nickel chloride ($NiCl_2{\cdot}6H_2O$) was measured in a 50 ml glass beaker, whereas 2.99 g (3 M) of

sodium hydroxide (NaOH) was measured in 25 ml beaker. Different concentrations of precursors are used to get the variety of nickel ferrite nanoparticles. Different masses of nickel ferrite are used like 0.025, 0.0259, 0.077, 0.0103 g and ferric chloride like 3.18, 3.114, 3.05, 2.98 g for 2, 4, 6 and 8% nickel ferrite nanoparticles respectively, Sodium hydroxide was dropped in the solution of the ferric chloride and nickel chloride drop wise for 40 min at the constant temperature of 80 °C with constant stirring on magnetic stirrer shown in Fig. 3a. The pH of the solution should be >12. Filter the prepared precipitate by filter paper and dried by constant temperature oven by overnight. After drying precipitates were annealed at 600 °C for 6 h. Then we get magnetic nickel ferrite nanoparticles with the variety of nickel concentration.

Experimental setup and experimental steps to complete the synthesis of the pure ferrite and nickel ferrite nanoparticles in the lab is as shown in Fig. 3.

3 Characterizations

The prepared magnetic samples were characterized by the powder X-ray diffraction (XRD), scanning electron microscopy (SEM), ultra-violet visible spectroscopy (UV–Vis) and Fourier-transform infrared spectrometer (FTIR).

X-ray powder diffraction (XRD) with source copper Cu-k_α of wavelength 1.5406 Å with 60 kV/30 mA to examine the crystal structural properties as well as the grain size [49–52] and phase identification [53]. The prepared samples were placed into diffractometers and start to run and collect data continuously. The size of the nanoparticles are calculated by the Debye–Scherrer's formula [54] that is in Eq. 1.

$$D = \frac{0.9\lambda}{\beta \cos\theta} \tag{1}$$

where, λ is the wave length of X-ray used which is 1.5406 Å [22]. β is the full width of half maxima of the peak. θ is the diffraction angle of X-ray for the planes *hkl*. Scanning electron microscopy (SEM) is the characterization tool which gives the size and morphology analysis with the help of imaging of the sample at different resolution. In this work imaging are taken by the SEM at 50 µm resolution and analyze the ranging of the particle size of the pure ferrite and the nickel ferrite at different concentrations. These samples are characterized with SEM system at applied voltage 15 kV. SEM tells us about the size range of the nanoparticles. Ultra-violet visible spectroscopy (UV–Vis) is the technique to study the optical properties of the material synthesized by the co-precipitation method in this work. This includes the study of the absorbance of the synthesized nanoparticles with different concentration of nickel, corresponding to the wavelength of the ultra-violet and visible light ranging from 200 to 500 nm and the absorption rang is 0–0.15. As wavelength of the light is along the horizontal axis (Y-axis) and absorbance of the material is along the vertical axis (X-axis). Fourier-transform infrared spectrometer (FTIR) is the study of the transmittance of the nanoparticles under the influence of infrared radiations (IR)

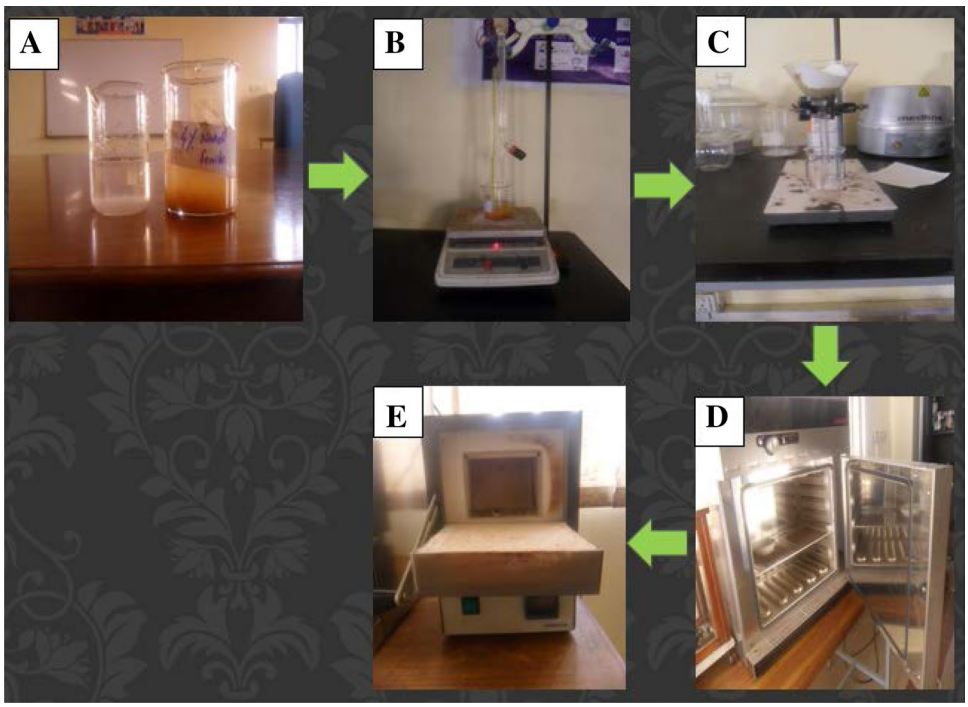

Fig. 3 Experimental setup. **a** Solution, **b** drop wise addition of sodium hydroxide, **c** filtration, **d** drying, **e** annealing

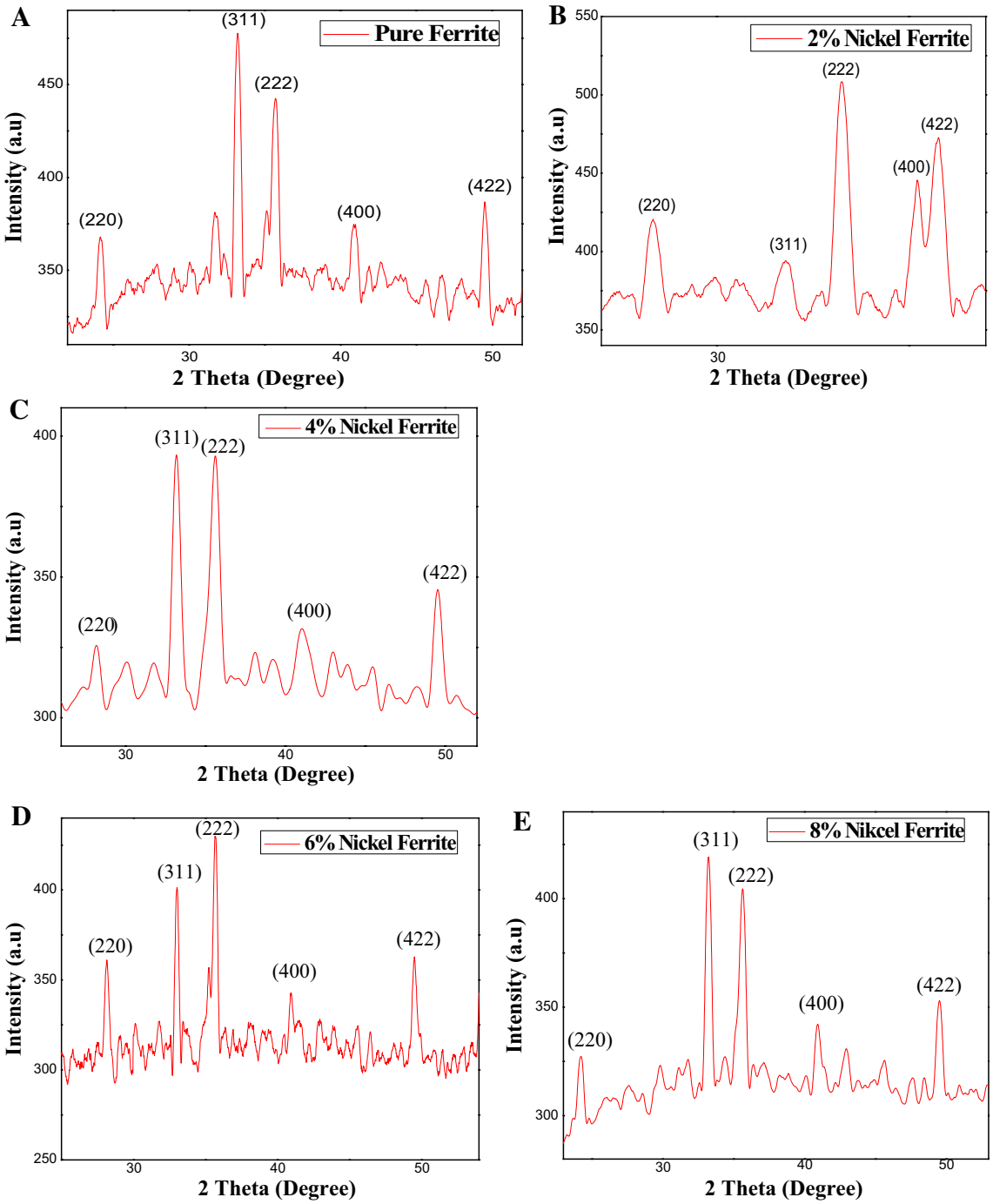

Fig. 4 X-ray diffraction analysis. **a** Pure ferrite, **b** 2%, **c** 4%, **d** 6%, **e** 8% nickel ferrite nanoparticles

[55]. In this case we study the transmittance of the pure ferrite and nickel ferrite nanoparticles. In the graphical explanation on vertical axis is representing the percentage transmittance and the other horizontal axis is representing by the wavenumber of the IR radiations. The selected range of the wave number is 400–4500 cm^{-1} and the selected range of the percentage transmission along vertical axis is 50–100%.

4 Results and Discussion

4.1 Powder X-Ray Diffraction (XRD) Analysis

The crystal structures of the magnetic particles are studied by the XRD. The data given by the XRD is manipulated to calculate the miller indices of the crystal phases and shown by the peaks on the graph. The peaks observed

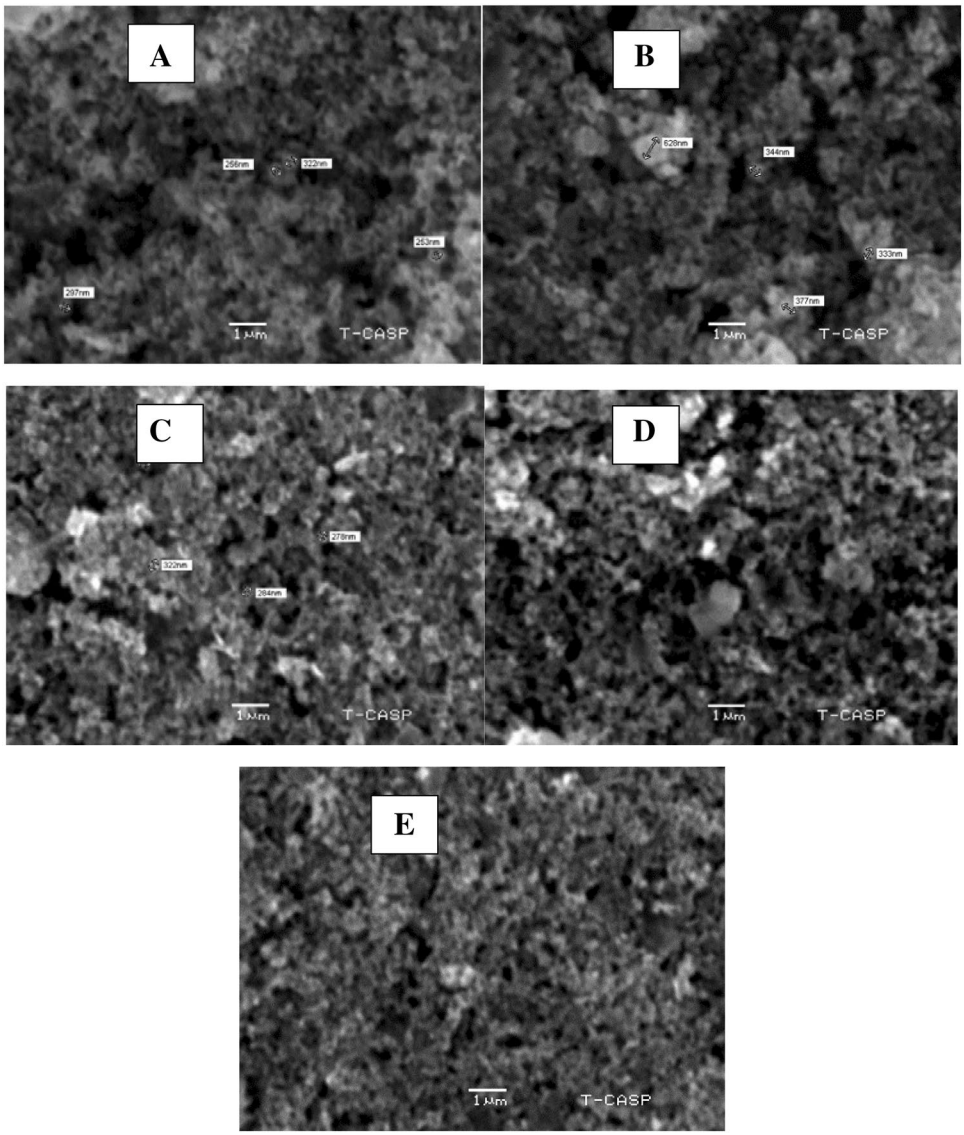

Fig. 5 SEM analysis of pure and nickel ferrite nanoparticles

by the XRD are compared with the Joint Committee Powder Diffraction Standards (JCPDS) [56] data card No. 01-086-2267 for the identification of phase which showed the phases (220), (311), (222), (400) and (422).

Figure 4 shows the XRD peaks of synthesized nanoparticles with different concentration of the nickel. The miller indices are the special indication for the existence of spinal cubic structure of nickel ferrite nanoparticles with the lattice parameter 8.393 Å which indicate the presence of the additional phases which are hematite Fe_2O_3 or NiO. The peaks on the graph are shifted backward with the lighter variation in the concentration of nickel. This indicates that the size of the nickel ferrite nanoparticles is proportional to the nickel concentration. The calculated particle size of the nanoparticles of nickel ferrite increases within the range of 40–60 nm.

4.2 Scanning Electron Microscope Analysis (SEM)

Images of the SEM of synthesized nanoparticles with wet chemical co-precipitation method with different concentrations of the nickel are shown in Fig. 5. Figures are named as a, b, c, d and e which are representing the pure ferrite, 2, 4, 6 and 8% nickel ferrite nanoparticles respectively.

The size of the nickel ferrite nanoparticles is ranging from 250 to 400 nm by scaling method with uniform morphology appearance with little bit agglomeration. The addition of nickel causes the formation of NiO and Fe_2O_3 from FeO which causes the increase in grain size of the nickel ferrite nanoparticles. As this results that the grain size is proportional to the amount of nickel.

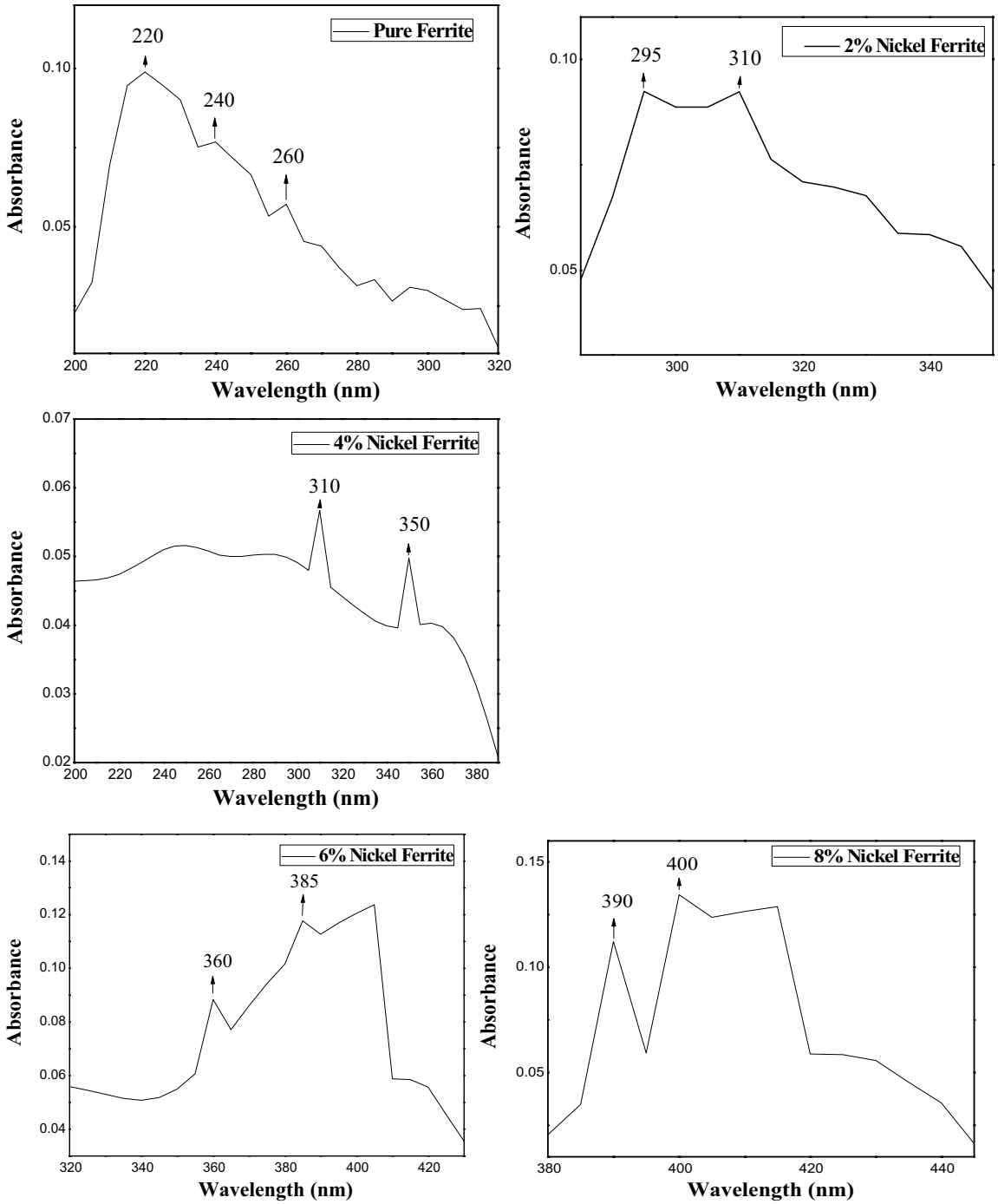

Fig. 6 UV–Vis spectrometry analysis of nickel ferrite with different concentrations

4.3 Ultra-Violet Visible Spectroscopy Analysis

The results of UV–Vis characterization are shown in Fig. 6. The graphical representation shows the variation in absorption of pure and nickel ferrite nanoparticles.

UV–Vis shows the red shift within the range of 200–400 nm of absorption peaks by increasing the concentration of nickel in ferrite. Red shift causes to decrease the band gape and increase in particle size. So by increasing the concentration of nickel the band gape of the atoms decreases and particle size increases.

4.4 Fourier-Transform Infrared Spectrometry Analysis

The graphical spectra of FTIR for pure and nickel ferrite nanoparticles with the variety of concentration are shown

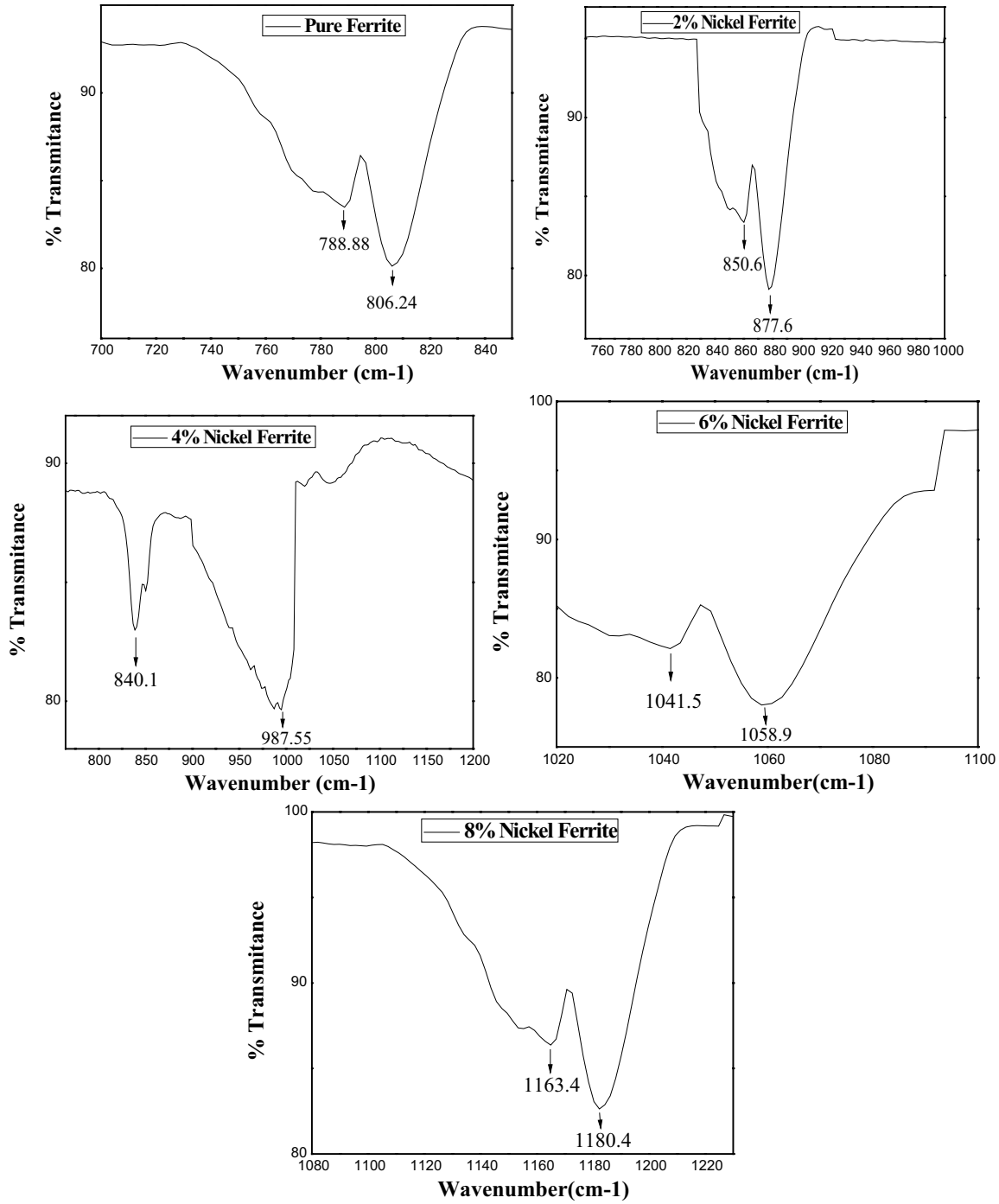

Fig. 7 Fourier-transform infrared spectrometry analysis of nickel ferrite with different concentrations

in Fig. 7. It is concluded that the transmittance peak is shifted forward by the increases in the concentration of the nickel. It is also observed that the bands of oxygen with any metal used in the samples are scanned within the range of the 400–1000 cm^{-1} which point out the existence of the ferrite and nickel ferrite nanoparticles.

Vibrational bands of the iron and nickel are observed within the range of wavenumber 1000–1200 cm^{-1} is the region of the vibrational bands of Fe_2O_3 in octahedral site and Ni–O in tetrahedral sites present in the samples. The transmittance peaks shift forward because the addition of nickel. Nickel creates the bonding with oxygen by which

vibrational mode of the sample increases which becomes the cause of the shifting of the peaks. The blurred portion of the graph shows that the greater amount of transmission of IR radiation so there will be no absorption within the blurred portion of the IR spectrum.

The results of all the characterization techniques are linked. XRD and SEM both show the grain size is directly proportional to the amount of nickel present in nickel ferrite. The red shifting in UV–Vis shows the decrease in band gap which indicates the increase in grain size. Similarly forward shifting of peaks in FTIR indicates the increase in the vibrational modes of Fe_2O_3 and NiO which shows the increase in grain size and transmission by increasing the amount of nickel. All the characterization techniques indicate the increase in size by increasing nickel in ferrite.

5 Conclusion

Nickel ferrite nanoparticles were prepared with different concentrations of the nickel. It is noted that properties of the prepared samples are dependent on the concentration of the nickel added in ferrite nanoparticles. XRD results show that the particle size increases with the increase in the concentration of the nickel in ferrite. It is also concluded that the crystal structure of the nickel ferrite nanoparticle is converted from face centered cubic structure to body centered cubic structure by the addition of nickel. The FTIR study concluded that transmission peaks are shifted forward by increasing the amount of the nickel. It is showed direct relation of transmission and amount of nickel. The UV–Vis shows red shift of the light which is the direct indication of the inverse effect on the band gape. The SEM analysis depicts that the increase in size of the nickel ferrite nanoparticles by increasing the concentration of the nickel. This study is useful to fabricate devices intended to store data, for the classification of inorganic materials which plays a very important role in the different aspects of life due to their outstanding magnetic, electronic and optical properties.

References

1. M. Dariel, L.H. Bennett, D.S. Lashmore, J. Appl. Phys. **61**, 4067 (1987)
2. W.D. Williams, N. Giordano, Phys. Rev. B **33**, 8146 (1986)
3. T.M. Whitney, J.S. Jiang, P.C. Searson, Science **261**, 1316 (1986)
4. L. Piraux, J.M. George, J.F. Despres, C. Leroy, Appl. Phys. Lett. **65**, 2484 (1994)
5. J. Yang, S.B. Park, H.G. Yoon, Y.M. Huh, S. Haam, Int. J. Pharm. **324**, 185–190 (2006)
6. F.X. Hu, K.G. Neoh, E.T. Kang, Biomaterials **27**, 5725–5733 (2006)
7. Y.L. Luo, L.H. Fan, F. Xu, Y.S. Chen, C.H. Zhang, Q.B. Wei, Mater. Chem. Phys. **120**, 590–597 (2010)
8. K.V.P.M. Shafi, Y. Koltypin et al., J. Phys. Chem. B **101**, 6409 (1997)
9. M. Khaldi, A. Benyoucef, C. Quijada, A. Yahiaoui, E. Morallon, J. Inorg. Organomet. Polym. Mater. **24**, 267–274 (2014)
10. Z. Cai, C.R. Martin, J. Am. Chem. Soc. **111**, 4138 (1989)
11. S.K. Chakarvarti, J. Vetter, Nucl. Instrum. Methods Phys. Res. B **62**, 109 (1991)
12. S.K. Chakarvarti, J. Vetter, J. Micromech. Microeng. **3**, 57 (1993)
13. S. Larumbe, C.G. Polo, J.I.P. Landazábal, A.G. Prieto, J. Nanosci. Nanotechnol. **12**, 1–9 (2012)
14. S. Benykhlef, A. Bekhoukh, R. Berenguer, E. Morallon, Colloid Polym. Sci. **294**, 1877–1885 (2016)
15. I. Radja, H. Djelad, E. Morallon, A. Benyoucef, Synth. Met. **202**, 25–32 (2015)
16. M. Kooti, A.N. Sedeh, J. Mater. Sci. Technol. **29**, 34–38 (2013)
17. F.S. Tehrani, V. Daadmehr, A.T. Rezakhani, J. Supercond. Novel Magn. **25**, 2443–2455 (2012)
18. M.H. Sousa, F. Augusta, J. Phys. Chem. **105**, 1168–1175 (2001)
19. F. Chouli, I. Radja, E. Morallon, A. Benyoucef, Polym. Compos. (2015)
20. R. Galindo, E. Mazario, S. Gutiérrez, M.P. Morales, P. Herrasti, J. Alloys Compd., **536S**, S241–S244, (2012)
21. G. Fan, Z. Yang, L. Li, J. Chem. Eng. **155**, 534 (2009)
22. S.Y. Vilar, M.S. Andujar, C.G. Aguirrea, J. Mira, M.A.S. Rodrıguez, J. Solid State Chem. **182**, 2685–2690 (2009)
23. R.H. Kodama, J. Magn. Magn. Mater. **200**, 359 (1999)
24. S. Prasad, N.S. Gajbhiye, J. Alloys Compd. **265**, 87 (1998)
25. S. Son, M. Taheri, E. Carpenter, J. Appl. Phys. **91**, 7589 (2002)
26. F.Z. Dahou, M.A. Khaldi, A. Zehhaf, A. Benyoucef, M.I. Ferrahi, Adv. Polym. Technol. **35**, 1–8 (2016)
27. S.K.E. Islam, P. Sharma, J. Nano Electron. Phys. **6**, 1–4 (2014)
28. R. Asokarajan, A.M.F. Benial, K. Neyvasagam, Int. J. Nanosci. Nanotechnol. **4**, 113–120 (2013)
29. P.H. Gomez, J.M. Munoz, M.A. Valente, C. Torres, C. de Francisco, Eur. Phys. J. Conf. **40**, 170031–170034 (2013)
30. V.R. Cosovic, N.M. Talijan, A.R. Cosovic, J. Trends Dev. Mach. Assoc. Technol. **18**, 115–118 (2014)
31. R. Suresh, P. Moganavally, M. Deepa, Int. J. ChemTech Res. **8**, 113–116 (2015)
32. Z.P. Cherkezova-Zheleva, K.L. Zaharieva, V.S. Petkova, B.N. Kunev, I.G. Mitov, Bulg. Chem. Commun. **44**, 24–29 (2012)
33. K. Maaz, S. Karim, S.K. Mumtaz, Hasanain, J. Liu, L. Duan, J. Magn. Magn. Mater. **321**, 1838–1842 (2009)
34. A. Gatelyte, D. Jasaitis, A. Beganskiene, A. Kareiva, Mater. Sci. **17**, 302–307 (2011)
35. S. Omprakash, A.S. Roy, P.S. Naik, Int. J. Basic Appl. Res. **1**, 17–23 (2011)
36. K. Rafeekali, M. Maheem, E.M. Mohammed, Int. J. Eng. Sci. Innov. Technol. **4**, 194–198 (2015)
37. E. Perez, C.G. Polo, S. Larumbe, J.I.P. Landazabal, V. Sagredo, Revista Mexicana de Fisica S, **58**, 104–107 (2012)
38. M.P. Reddy, W. Madhuri, K. Sadhana, J. Sol-Gel. Sci. Technol. **70**, 400–404 (2014)
39. B.P. Jacob, A. Kumar, R.P. Pant, S. Singh, E.M. Mohammed, Bull. Mater. Sci. **34**, 345–1350 (2011)
40. K. Nejati, R. Zabihi, Chem. Cent. J. **6**, 1–6 (2012)
41. S. Diodati, L. Pandolfo, A. Caneschi, S. Gialanella, Nano Res. **7**, 1027–1042 (2014)
42. N. Kasapoglu, A. Baykal, M.S. Toprak, Y. Koseoglu, H. Bayrakdar, Turk. J. Chem. **31**, 659–666 (2007)
43. F. Chouli, A. Zehhaf, A. Benyoucef, Macromol. Res. **22**, 26–31 (2014)

44. Z.H. Zhou, J.M. Xue, J. Wang, J. Appl. Phys. **91**, 6015–6020 (2002)
45. R. Gopal, S.C. Singh, R.K. Swarnkar, Nano Sci. Technol. Inst. **1**, 166–169 (2009)
46. H. Kavas, N. Kasapoglu, A. Baykal, Y. Koseoglu, Chem. Pap. **63**, 450–455, (2009)
47. H.R. Ghorbani, A.A. Safekordi, H. Attar, S.M. Rezayat Sorkhabadi, Chem. Biochem. Eng. Q. **25**, 317–326 (2011)
48. A.B. Seabra, N. Durán, Metals **5**, 934–975 (2015)
49. P.S. Foner, Rev. Sci. Instrum. **30**, 548–557 (1959)
50. C. Suryanarayana, M.G. Norton, *X-Ray Diffraction: A Practical Approach*, 1st edn. (Springer Science + Business Media, New York, 1998)
51. A.R. West, *Basic Solid State Chemistry*, 2nd edn. (Wiley, New York, 1987)
52. A. Dey, A.K. Mukhopadhyay, S. Gangadharan, M.K. Sinha, J. Therm. Spray Technol. **18**, 578 (2009)
53. J. Singh, M. Srivastava, A. Roychoudhury, D.W. Lee, S.H. Lee, B.D. Malhotra, J. Phys. Chem. B **117**, 141 (2013)
54. S. Kumar, P. Sharma, V. Sharma, J. Appl. Phys. **111**, 113510 (2012)
55. R. Asokarajan, Int. J. Nanosci. Nanotechnol. **4**, 113–120 (2013)
56. R. Das, M.E. Ali, S.B.A. Hamid, Rev. Adv. Mater. Sci. **38**, 95–109 (2014)